

SUG-Occ: An Explicit Semantics and Uncertainty Guided Sparse Learning Framework for Real-Time 3D Occupancy Prediction

Hanlin Wu¹, Pengfei Lin¹, Member, IEEE, Ehsan Javanmardi¹, Nanren Bao, Bo Qian¹, Member, IEEE, Hao Si¹, Manabu Tsukada¹, Member, IEEE

Abstract—As autonomous driving moves toward full scene understanding, 3D semantic occupancy prediction has emerged as a crucial perception task, offering voxel-level semantics beyond traditional detection and segmentation paradigms. However, such a refined representation for scene understanding incurs prohibitive computation and memory overhead, posing a major barrier to practical real-time deployment. To address this, we propose SUG-Occ, an explicit Semantics and Uncertainty Guided Sparse Learning Enabled 3D Occupancy Prediction Framework, which exploits the inherent sparsity of 3D scenes to reduce redundant computation while maintaining geometric and semantic completeness. Specifically, we first utilize semantic and uncertainty priors to suppress projections from free space during view transformation while employing an explicit unsigned distance encoding to enhance geometric consistency, producing a structurally consistent sparse 3D representation. Secondly, we design an cascade sparse completion module via hyper cross sparse convolution and generative upsampling to enable efficiently coarse-to-fine reasoning. Finally, we devise an object contextual representation (OCR) based mask decoder that aggregates global semantic context from sparse features and refines voxel-wise predictions via lightweight query–context interactions, avoiding expensive attention operations over volumetric features. Extensive experiments on SemanticKITTI benchmark demonstrate that the proposed approach outperforms the baselines, achieving a 7.34% improvement in accuracy and a 57.8% gain in efficiency. Code and models are available at <https://github.com/tlab-wide/SUGOcc>.

Index Terms—Semantic Occupancy Prediction, Sparse Learning, Autonomous Driving, Scene Understanding, Vision Centric Perception

I. INTRODUCTION

THE 3D semantic occupancy prediction has emerged as an fundamental perception task for scene understanding in autonomous driving, thanks to its ability to jointly estimate voxel-level geometric and semantic states in 3D space [1]. Differing from conventional perception paradigms like image segmentation [2], [3], bounding-box detection [4], [5], and

This work was supported by the JST ASPIRE Program (Grant Number JPMJAP2325), JST CRONOS (Grant Number JPMJCS24K8) and JST SPRING (Grant Number JPMJSP2108). (Corresponding author: XXX)

Hanlin Wu, Pengfei Lin, Ehsan Javanmardi, Nanren Bao, Hao Si, Manabu Tsukada are with the School of Information Science and Technology, The University of Tokyo, 1-1-1, Yayoi, Bunkyo-ku, Tokyo, 113-8657 Japan. (e-mail: {hanlinwu, linpengfei0609, ejavanmardi, naren, si-hao, mtsukada}@g.ecc.u-tokyo.ac.jp)

Bo Qian is with the Information Systems Architecture Science Research Division, National Institute of Informatics, Tokyo 101-8430, Japan (e-mail: boqian@ieee.org)

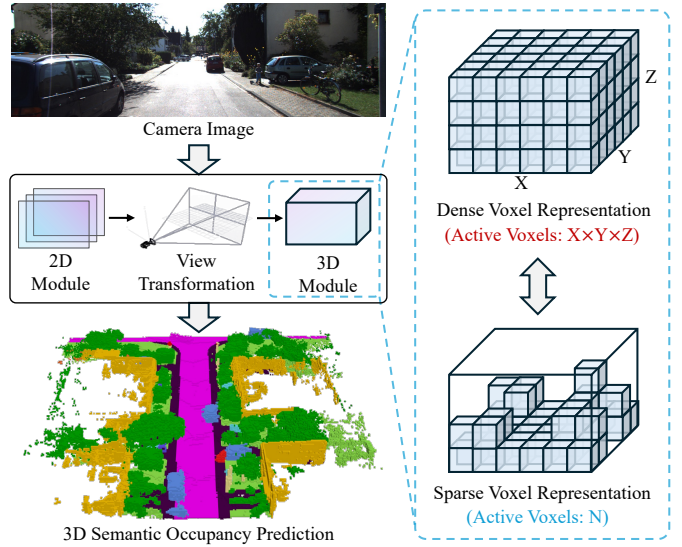


Fig. 1: Illustration of the inherent sparsity of 3D semantic occupancy prediction.

Bird-Eye-View (BEV) map [6], [7], 3D semantic occupancy prediction produce dense and spatially consistent 3D scene representations which is beneficial for downstream tasks such as motion planning and other safety-critical decision-making in real-time autonomous systems.

Despite these advantages, 3D semantic occupancy prediction poses a critical computational bottleneck for real-time deployment. Most existing approaches follow a two-stage pipeline, where multi-view image features are first lifted into a 3D volume via view transformation, typically based on Lift-Splat-Shoot (LSS) [8] or transformer-driven BEV mapping [6], and then processed by dense 3D Convolutional Neural Networks (CNNs) or transformer decoders. While effective, this design leads to substantial memory overhead and inference latency due to the massive intermediate feature space. Even a 3D volume with moderate spatial resolution contains hundreds of thousands locations.

At the core of the inefficiency lies a fundamental mismatch between dense computation and the inherently sparse nature of real-world 3D environments. In typical autonomous driving scenes, only a small fraction of voxels correspond to physical

objects, while the overwhelming majority represent free space. Nevertheless, existing occupancy prediction methods allocate equal computational resources to all voxels, i.e., occupied or empty, resulting in substantial redundancy. Consequently, a significant portion of the computational budget is wasted on voxels that contribute little to perception quality. This structural inefficiency presents a major roadblock to deploying semantic occupancy prediction in real-time autonomous driving systems.

Driven by this sparsity imbalance, recent works like SparseOcc [9] and Pasco [10] have explored the promise of introducing sparse representations into the occupancy prediction pipeline by exploiting the natural sparsity that emerges from Lidar scans or from the geometric misalignment between camera rays and voxel centers during the Lift-Splat-Shoot (LSS) projection. While this reduces the number of active voxels, the resulting sparsity is incidental rather than principled, which stems from projection geometry rather than the semantic structure of the scene. As a result, numerous voxels corresponding to free space or uncertain projections remain within the sparse volume, continuing to consume computational resources with limited perceptual value.

More critically, existing sparse methods [11] [12] often lack high-level image priors when deciding which voxels to retain or discard. Depth distributions are typically predicted, but only used as projection weights during view transformation, which are often sharply peaked around visible surfaces, providing limited expressiveness along the camera ray. Furthermore, high-level semantic priors are entirely decoupled from the lifting process and are not exploited to suppress semantically implausible or free-space projections [9]. As a result, unreliable or semantically implausible projections contaminate the 3D feature space, undermining the intended benefits of sparsity. The pipeline still ends up processing many voxels that offer little to no geometric insight. This not only degrades the representational quality of sparse volumes, but also introduces computational waste, posing a major barrier to real-world deployment of sparse occupancy prediction systems.

To address the limitations of existing 3D semantic occupancy prediction methods, we propose SUG-Occ, a real-time semantic occupancy framework that leverages explicit semantics and uncertainty guided sparse learning to reduce computational cost while enhancing geometric and semantic consistency. To be specific, in order to obtain a cleaner and more informative sparse 3D representation, we introduce a semantics and uncertainty guided LSS module to selectively project image features into 3D space based on the semantic and depth uncertainty priors rather than indiscriminately lifting all image features. In addition, to efficiently perform the coarse-to-fine geometric and semantic reconstruction over the sparse 3D representations, we design a cascade sparse completion network, which progressively expands active voxels via generative upsampling, efficiently refines structural voxels using hyper-cross sparse convolutions, and adaptively prunes low-confidence regions to tightly control computational overhead. Furthermore, for final semantic occupancy predictions, we propose a lightweight OCR based mask decoder that derives object contextual representations from sparse voxel features

and restricts query interactions to this compact context, avoiding dense voxel-wise attention operations. A global OCR embedding is also maintained and updated via weighted accumulation, providing a global semantic prior with negligible overhead.

In summary, the contributions of this work are three folds:

- We introduce a semantics and uncertainty guided LSS module to select informative image projections and incorporate an explicit distance encoding, producing a geometrically and semantically coherent sparse 3D representation with controllable active voxels.
- We design a cascade sparse completion network that enables efficient coarse-to-fine occupancy completion over sparse voxels via hyper-cross sparse convolution, generative upsampling and adaptive pruning.
- We propose a OCR based mask decoder to efficiently refine semantic occupancy prediction, which aggregate object context from sparse features, maintain global context and perform only query-context interactions, avoiding multi-scale and dense voxel-wise attention.

Extensive experiments on SemanticKITTI dataset demonstrate that the proposed framework validate the superiority of the proposed approach over baselines, yielding a 7.34% accuracy improvement and a 57.8% efficiency enhancement.

II. RELATED WORK

A. 2D-to-3D View Transformation

Transforming image features into structured 3D representations is a fundamental component of vision-based 3D perception in autonomous driving. Existing methods can be broadly divided into explicit and implicit view transformation paradigms. In explicit view transformation, the pioneering LSS [8] introduced a dominant paradigm: it predicts a discrete depth distribution for each pixel and explicitly lifting image features into a 3D frustum. Due to its geometric interpretability and efficiency, LSS has served as the foundation for a wide range of BEV-based detection and perception systems [13], [14], [15]. Subsequent extensions such as BEVDepth [16] further enhanced this paradigm by incorporating camera-aware modeling and explicit depth supervision.

In contrast, implicit view transformation learns pixel-to-3D correspondences directly through attention-based mechanisms without relying on explicit depth estimations. Representative methods include BEVFormer [6], which performs deformable cross-attention between BEV queries and image features. Building on this, SurroundOcc [17] extends this formulation from BEV representations to semantic occupancy predictions. Together, explicit and implicit view transformation paradigms provide two dominant approaches for constructing 3D representations from 2D images and form the foundation of modern BEV and voxel-based perception systems.

B. 3D Semantic Occupancy Prediction

3D semantic occupancy prediction aims to jointly infer the occupancy status and semantic category of each voxel in a 3D scene, offering a unified representation of geometry and

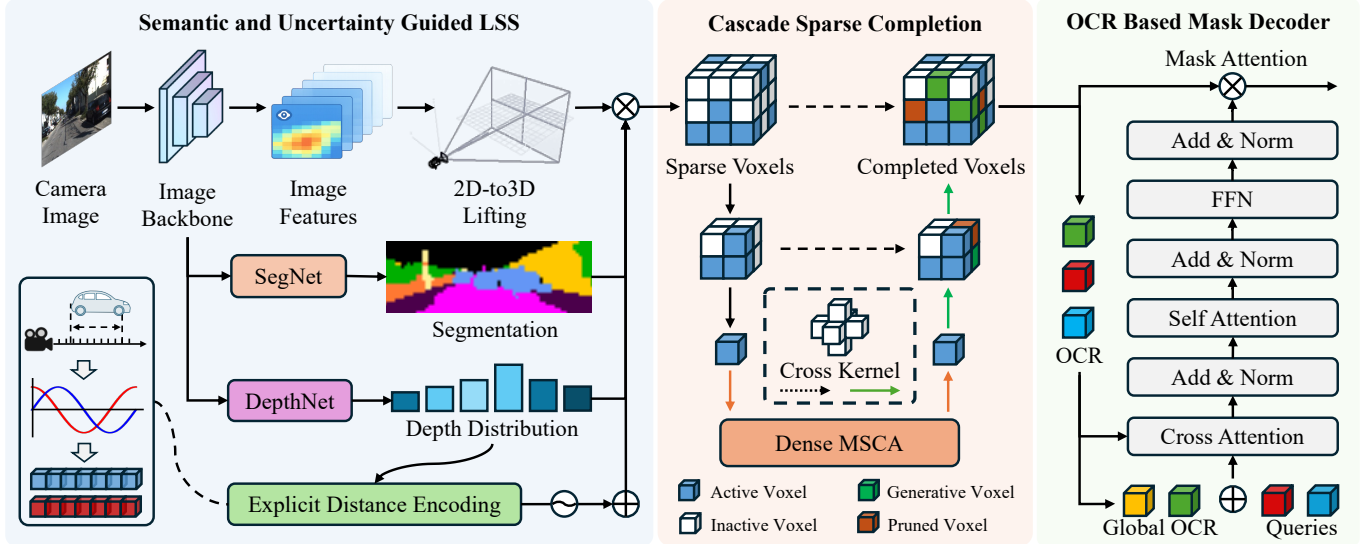


Fig. 2: Overview of the proposed SUG-Occ framework. At first, image features extracted from a single-frame camera input are selectively lifted into 3D space using semantic and depth uncertainty priors, yielding a sparse and structurally coherent initialization with explicit distance encoding. Then, an efficient cascade sparse completion network progressively reconstructs geometry and semantics while tightly controlling computational cost through generative upsampling and soft pruning. Finally, an OCR-based mask decoder further refines predictions by restricting attention to compact object contextual representations.

semantics. This task was first introduced by SSCNet [18], which predicts complete 3D semantic scenes from single-view depth image in indoor environments. With the advent of large-scale datasets such as SemanticKITTI [19], [20], SSCBench [21], and Occ3D [22], semantic occupancy prediction has been extended to complex outdoor scenarios in autonomous driving.

Early works on semantic occupancy prediction predominantly relied on LiDAR-based inputs due to their accurate geometric measurements. Representative approaches such as LMSCNet [23], S3CNet [24] and JS3CNet [25] demonstrated the effectiveness of volumetric reasoning for reconstructing dense 3D semantics from sparse point clouds.

More recently, vision-centric semantic occupancy prediction has gained increasing attention due to its strong potential and lower deployment cost in autonomous driving. Methods like MonoScene [26], SurroundOcc [17], OccFormer [27], VoxFormer [28], SparseOcc [9], GEOcc [29], ALOcc [30] and ProtoOcc [31], have progressively advanced the capability of vision-based models to infer high-quality 3D semantic occupancy predictions from multi-view images. Despite these advances, vision-based semantic occupancy prediction remains fundamentally challenged by depth ambiguity, noisy or inconsistent view transformation, and the high computational overhead required for real-time deployment.

C. Sparse Learning for 3D Perception

Offering an efficient paradigm by operating only on active positions and avoiding redundant computation inherent in dense representations, sparse learning [32], [33], [34] is widely used by Lidar-based perception system, where the natural sparsity of point clouds aligns well with the sparse computational model. Representative approaches [4], [35] and subsequent

variants [36], [37] demonstrated that sparse 3D architectures can effectively support large-scale real-time perception.

However, directly transferring sparse learning to camera-based perception is non-trivial due to the inherently dense nature of multi-view image inputs. To bridge this gap, recent works have explored introducing sparsity into the vision-based 3D perception. For instance, SparseBEV [38] proposes sparse BEV representations with token selection strategy for 3D object detection, while PointBEV [39] lifts multi-view image features into sparse point-based representations and perform 3D reasoning on sampled keypoints. Nevertheless, the sparsity patterns in these approaches are largely driven by heuristic sampling or attention-based relevance estimation, and lack explicit geometric and semantic grounding, which is crucial for semantic occupancy prediction.

III. METHODOLOGY

In this section, we introduce the proposed framework for real-time 3D semantic occupancy prediction that leverages explicit semantics and uncertainty guided sparse learning.

A. Problem Formulation

We formulate the task as predicting a voxel-wise semantic occupancy field of a 3D driving scene from a set of calibrated camera images. Given input images $I \in \mathbb{R}^{N \times H \times W \times 3}$ captured by N cameras where H and W denote the image height and width, respectively. Each camera is associated with an intrinsic matrix $K \in SE(3)$ and an extrinsic pose $T \in SE(3)$. The objective is to infer a 3D semantic occupancy grid $Occ \in \mathbb{R}^{X \times Y \times Z}$, where X , Y , and Z denote the spatial dimensions of the voxel grid along the longitudinal, lateral, and vertical axes. Each voxel in Occ represents the semantic category of

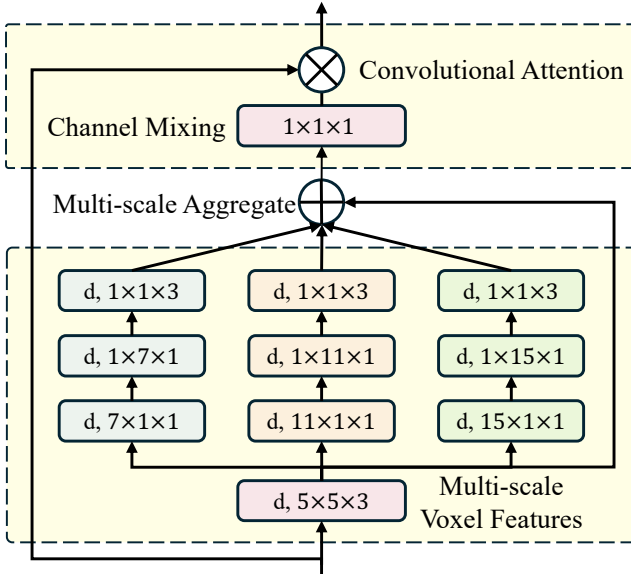


Fig. 3: Illustration of the multi-scale convolutional attention, which is consist of multi-scale decomposed depth-wise convolution for context aggregation, a point-wise convolution for channel mixing and a convolutional attention for residual operation.

its corresponding spatial location, including free space as well as object categories like car, pedestrian, and vegetation.

B. Overview

The proposed framework follows a three-stage pipeline for 3D semantic occupancy prediction. Given the input images, we first apply a **Semantics and Uncertainty Guided LSS** to obtain a clean and structurally plausible initial 3D sparse feature volume. Instead of indiscriminately projecting all image features into the voxel grid, this module leverages semantic priors and depth-based uncertainty estimation to filter out unreliable projections and suppress high-confidence free-space regions before lifting into 3D domain. Then, an efficient **Cascade Sparse Completion Network** processes the filtered 3D sparse feature volume using Minkowski sparse convolutions. This network performs 3D reasoning only on active voxels and progressively reconstructs geometric structures through generative upsampling, while adaptively pruning semantically implausible locations to tightly control computational overhead. Finally, an **OCR-based Mask Decoder** aggregates global semantic context from the sparse voxel features and refines voxel-wise predictions via a query–context interaction mechanism. By restricting attention operations to compact contextual representations, the proposed framework produces the final dense semantic occupancy field with significantly reduced computational overhead.

C. Explicit Semantics and Uncertainty Guided LSS

The view transformation step plays a crucial role in determining the quality of the initial 3D feature volume. However, standard LSS pipelines indiscriminately lift all image features

into the voxel space, regardless of their semantic relevance or geometric reliability. As a result, regions corresponding to free space are still projected, introducing substantial noise and redundancy in 3D domain. To address this issue, we propose a explicit semantics and uncertainty guided LSS mechanism that selectively removes redundant projections in view transformation and enhances geometric consistency via explicit distance encoding.

Given the input images, we extract the multi-scale image features using a shared image backbone (e.g., ResNet-50), followed by feature pyramid fusion to obtain a downsampled image feature map $F \in \mathbb{R}^{H_d \times W_d \times C}$, which serves as the input to the LSS module. Based on this image feature map, we perform two auxiliary predictions, a semantic segmentation $F_{sem} \in \mathbb{R}^{H_d \times W_d \times S}$ and a depth distribution $F_{depth} \in \mathbb{R}^{H_d \times W_d \times D}$, where S and D denote the number of semantic classes and discretized depth bins, respectively.

For each pixel (h, w) , we obtain the semantic probability $P_{sem}(h, w) \in \mathbb{R}^S$ and the depth probability distribution $P_{depth}(h, w) \in \mathbb{R}^D$ via a softmax operation. The semantic segmentation provides a measure of whether a pixel corresponds to a physically meaningful structure in the 3D scene. Assuming that class 0 represents free space, we define the non-empty probability of a pixel as

$$P_{nonempty}(h, w) = 1 - P_{sem}(h, w, 0) \quad (1)$$

Furthermore, we quantify the geometric uncertainty of projected depths along each camera ray using the cumulative distribution of the predicted depth distribution. Specifically, for each pixel (h, w) and depth bin d , we define a cumulative depth confidence as

$$P_{uncertain}(h, w, d) = \sum_{i=0}^d P_{depth}(h, w, i) \quad (2)$$

which serves as a proxy for depth uncertainty. A low cumulative probability indicates an foreground-dominated depth bin, whereas a high value suggests a more ambiguous geometric estimate.

Together with the semantic prior, these two probabilities enable us to identify and discard ambiguous or low-quality image positions before lifting the image features into the 3D voxel space. We construct a binary mask that suppresses pixels with a high likelihood of belonging to free space or exhibiting unreliable geometric estimates.

$$Mask(h, w, d) = \begin{cases} 1, & \text{if } P_{nonempty}(h, w) > \tau_s \text{ and} \\ & P_{uncertain}(h, w, d) > \tau_d, \\ 0, & \text{else.} \end{cases} \quad (3)$$

where τ_s and τ_d are predefined thresholds controlling semantic relevance and geometric reliability, respectively.

During view transformation, voxel features are computed only from masked-valid pixels, resulting in a significantly cleaner and more structurally coherent 3D initialization. By suppressing free-space and ambiguous projections at view transformation stage, the resulting 3D sparse feature volume provides a more reliable foundation for subsequent sparse 3D reasoning.

Moreover, unlike the original LSS formulation that aggregates feature using depth distribution probability as interpolation weights which often leads to geometric blurring under peak depth distribution, we introduce an explicit unsigned distance encoding to preserve geometric continuity along each camera ray. Instead of probabilistically spreading features across depth bins, we anchor features at the expected depth and encode their relative distance to each depth hypothesis. Specifically, given the depth probability distribution $P_{depth}(h, w, d)$, we estimate the expected depth as

$$E_{depth}(h, w) = \sum_{i=0}^D i \cdot P_{depth}(h, w, i) \quad (4)$$

where d and i denote discrete depth bin indices.

We then compute the unsigned distance the unsigned distance between each depth bin and the expected depth as

$$\Delta_{dist}(h, w, d) = |d - E_{depth}(h, w)| \quad (5)$$

This relative distance is embedded using a sinusoidal positional encoding, which is defined as

$$\begin{aligned} PE_{(h, w, d, 2i)} &= \sin(\Delta_{dist}(h, w, d) / T^{2i/C}) \\ PE_{(h, w, d, 2i+1)} &= \cos(\Delta_{dist}(h, w, d) / T^{2i/C}) \end{aligned} \quad (6)$$

where T is a temperature hyperparameter controlling the frequency scale.

Finally, the explicit distance encoding is added to the original image feature to form the lifting features, which is defined as

$$F'(h, w, d) = F(h, w) + PE_{(h, w, d)} \quad (7)$$

Based on the explicit distance embedded image features and the semantics and uncertainty guided mask, we obtain an initial sparse volume feature $V_0 \in \mathbb{R}^{X_{1/2} \times Y_{1/2} \times Z_{1/2} \times C}$, where $X_{1/2}, Y_{1/2}, Z_{1/2}$ denote the spatial dimensions at $1/2$ resolution with respect to the full voxel grid.

D. Cascade Sparse Completion

To efficiently perform 3D occupancy completion on the sparse feature volume produced by the semantics and uncertainty guided LSS module, we introduce an cascade sparse completion module, built upon a sparse generative 3D U-Net [35].

Specifically, the input sparse feature volume V_0 is processed by a sparse encoder consisting of submanifold sparse convolutions and sparse downsampling layers, producing multi-scale sparse volume features V_i , $i \in \{0, 1, 2, 3\}$ at resolution $s \in \{1/2, 1/4, 1/8, 1/16\}$. The coarsest feature volume V_3 at resolution $1/16$ serve as the bottleneck representation. To enhance multi-scale geometric context and enable geometry generation beyond the input sparse manifold, we employ a lightweight dense multi-scale convolutional attention (MSCA) module [2] on this bottleneck representation, as illustrated in Fig. 3. The MSCA-enhanced bottleneck feature is computed as

$$V'_3 = V_3 \otimes Conv_{1 \times 1 \times 1} \left(\sum_{i=0}^3 Scale_i(DW\text{-}Conv(V_3)) \right) \quad (8)$$

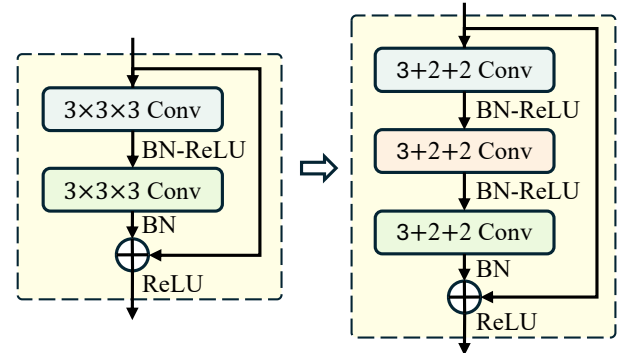


Fig. 4: Illustration of the proposed hyper cross residual block. Compared with the conventional residual block using two stacked $3 \times 3 \times 3$ sparse convolutions, hyper cross residual block apply a three layers $3+2+2$ hyper cross convolution stack.

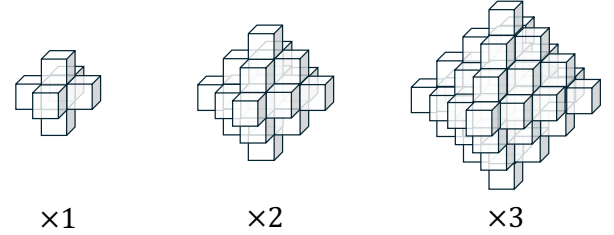


Fig. 5: Visualization of the receptive field expansion achieved by stacking hyper cross convolutions. As the number of layers increases, the effective receptive field progressively extends from axial neighbors to diagonal spatial locations.

where $DW\text{-}Conv$ denotes depth-wise convolution [40], $Scale_i$ denotes the i -th multi-scale branches, $Conv_{1 \times 1 \times 1}$ denotes point-wise convolution, and \otimes indicates element-wise multiplication.

On top of the bottleneck feature, we employ a cascade sparse generative decoder. At each decoding stage, features from the coarser scale are progressively upsampled via generative transpose convolution to activate new voxels. Following the U-Net paradigm, skip connections from the corresponding encoder stages are fused to preserve fine-grained geometric structures. In addition, we attach a lightweight semantic occupancy predictor as each stage to estimate a proxy semantic occupancy map $P_{occ,i}$, which provides informative supervision across multiple scales.

Guided by the predicted proxy semantic occupancy map, we perform a soft sparse pruning after each decoding stage to maintain sparsity for subsequent stages while preserving meaningful structures. Instead of hard pruning based on binary occupancy or semantic masks as commonly adopted in prior work, we only discard voxels with high confidence of being empty. Formally, we retain voxels whose predicted non-empty probability exceeds a threshold, which is defined as

$$V'_i = \{x \in V_i | P_{occ,i}(x) > \tau_p\} \quad (9)$$

where τ_p denotes the sparse pruning threshold.

Moreover, to further improve the computational efficiency, we adopt a hyper cross convolution kernel in both encoder and decoder. Unlike standard cubic convolution kernel, the hyper cross kernel aggregates features only from axial neighbors. For example, for an active voxel processed by a sparse convolution layer with kernel size 3, convolution is performed with only 6 axial neighbors instead of all 26 neighboring voxels. This design significantly reduces neighbor-matching operations and memory-access overhead, making sparse convolution more scalable and well-suited for real-time occupancy completion.

However, restricting convolution to axial neighbors inevitably limits the receptive field, particularly for diagonal or off-axis spatial interactions, which may hinder the propagation of contextual information in sparse volumes. To address this limitation, we modify the standard residual block by replacing the conventional two-layer design with a three-layer hyper cross sparse convolution stack as illustrated in Fig. 4. And as shown in Fig. 5, stacking three hyper cross convolution layers enables multi-hop feature propagation along axial directions, allowing the receptive field of a single residual block to effectively cover diagonal spatial regions. This design progressively expands spatial coverage while preserving the efficiency advantage of the hyper cross kernel, achieving a favorable balance between computational cost and contextual aggregation.

E. Object Contextual Representation Based Mask Decoder

To predict the final semantic occupancy result, we design an efficient query-based mask decoder inspired by recent mask-centric transformer models. Instead of performing expensive cross-attention between learnable queries and multi-scale voxel features, as commonly adopted in previous works, we rely on a compact object contextual representation (OCR) obtained from the sparse volume produced by the completion network.

Given the final sparse voxel feature V'_0 , we follow the formulation of OCRNet [41] to compute class-wise object contextual representation using the proxy semantic occupancy map $P_{occ,0}$. Specifically, $P_{occ,0}$ is treated as soft region assignment weights over active voxels, enabling the aggregation of sparse voxel features into class-level region embeddings. These embeddings encode semantic group-level context and provide a descriptor of the scene structure, which is defined as

$$R = \sum_{x \in V'_0} \text{Softmax}_x(P_{occ,0}(x)) \cdot V'_0 \quad (10)$$

where $R \in \mathbb{R}^{S \times C}$ denotes the object contextual representation of V'_0 and $\text{Softmax}_x(\cdot)$ denotes the softmax operation across active voxels.

In addition, we maintain a global OCR R_{global} to accumulate contextual representations over the course of training. After computing the OCR embeddings from current sparse feature volume, the global OCR is updated using an exponential moving average (EMA) strategy, which is defined as

$$R'_{global} = \alpha R_{global} + (1 - \alpha)R \quad (11)$$

where $\alpha \in (0, 1)$ denotes the momentum parameter.

Next, a set of learnable query embeddings $Q \in \mathbb{R}^{K \times C}$ interacts with the global OCR to retrieve a global contextual prior and attends to the current OCR through a cross-attention operation. By restricting attention interactions to a compact contextual space, this design substantially reduces computational overhead while retaining strong semantic reasoning capability, which is defined as

$$Q' = \text{Attn}(Q + R_{global}, R) \quad (12)$$

where K denotes the total amount of queries and $\text{Attn}(\cdot, \cdot)$ represents a standard multi-head cross-attention operator.

Afterwards, semantic scores and voxel masks are derived from the refined queries and the sparse feature volume. Specifically, each query predicts semantic logits and a mask embedding through linear projections. The semantic score $P_k \in \mathbb{R}^S$ is obtained via a softmax function, while a voxel mask $M_k \in \mathbb{R}^{X_{1/2} \times Y_{1/2} \times Z_{1/2}}$ is predicted by computing the dot product between the mask embedding and the sparse feature volume. The downsampled 3D semantic occupancy prediction is then obtained as

$$Occ_{1/2} = \sum_{k=1}^K P_k \cdot M_k \quad (13)$$

Finally, the full-resolution 3D semantic occupancy prediction is obtained through interpolation.

F. Training Objectives

Query DeNoising: To improve robustness of the model, we adopt a denoising training strategy following mask-based transformer frameworks [42]. Specifically, query embeddings and their corresponding ground-truth mask targets are perturbed during training, which stabilizes optimization and improves the association between queries and voxel masks.

Exponential Moving Average: To further stabilize model optimization and enhance generalization, we maintain an exponential moving average (EMA) [43] of all model parameters.

$$\theta_{EMA} = \beta \theta_{EMA} + (1 - \beta) \theta \quad (14)$$

where β denotes the momentum coefficient. This EMA mechanism operates independently of the global OCR, which instead accumulates contextual embeddings and serves as a semantic knowledge base.

Training Loss: The overall training loss \mathcal{L}_{total} is defined as

$$\mathcal{L}_{total} = \mathcal{L}_{depth} + \mathcal{L}_{seg} + \mathcal{L}_{prune} + \mathcal{L}_{cls} + \mathcal{L}_{mask} \quad (15)$$

where \mathcal{L}_{depth} and \mathcal{L}_{seg} denotes the binary cross-entropy (BCE) loss for depth estimation and cross-entropy (CE) loss for image semantic segmentation, respectively. \mathcal{L}_{cls} represents the CE loss for the semantic prediction of the refined queries. \mathcal{L}_{mask} is a combination of BCE loss and Dice loss for voxel mask. \mathcal{L}_{prune} corresponds to the multi-scale proxy semantic occupancy loss, which includes CE, Lovasz [44], and the geometric and semantic loss introduced in [26].

TABLE I: Overall 3D semantic occupancy prediction result on SemanticKITTI validation set. For each method, we report its venue, image backbone, parameter counts, geometry IoU, mean semantic IoU and FPS. * represents these methods are adapted for the image inputs, which are implemented and reported in MonoScene [26].

Method	Venue	Image Backbone	Params.	IoU	mIoU	FPS
LMSCNet* [23]	3DV'2020	-	-	28.61	6.70	-
3DSketch* [26]	CVPR'2020	-	-	33.30	7.50	-
AICNet* [45]	CVPR'2020	-	-	29.59	8.31	-
JS3C-Net* [25]	NeurIPS'2021	-	-	38.98	10.31	-
MonoScene [26]	CVPR'2022	EfficientNet-B7	-	37.12	11.50	-
TPVFormer [46]	CVPR'2023	ResNet-101	-	34.25	11.36	-
VoxFormer-S [28]	CVPR'2023	ResNet-50	-	44.02	12.35	-
OccFormer [27]	ICCV'2023	EfficientNet-B7	203.4M	36.50	13.46	4.1
SparseOcc [9]	ECCV'2024	EfficientNet-B7	229.9M	36.67	13.12	6.2
ProtoOcc [31]	AAAI'2025	EfficientNet-B7	167.0M	36.67	13.89	6.4
SUG-Occ (Ours)	-	ResNet-50	168.5M	35.87	14.92	10.1

IV. EXPERIMENTS

A. Dataset and Metrics

We evaluate the proposed method on the widely used SemanticKITTI dataset [19], which provides dense semantic occupancy annotations by augmenting LiDAR scans from KITTI Odometry Benchmark [47], which consists of 22 outdoor driving scenarios. Following the standard setting for semantic occupancy prediction on SemanticKITTI, the prediction region is defined as a fixed 3D volume centered at the ego vehicle. The predicted region covers $51.2m$ in front of the vehicle, $25.6m$ to both left and right sides and extents from $-2.0m$ to $4.4m$ along the vertical axis. This region is discretized into a voxel grid with a resolution of $256 \times 256 \times 32$, corresponding to a voxel size of $0.2 \times 0.2 \times 0.2m$. Each voxel is annotated with one of 20 classes, including 19 semantic categories and 1 free space class. In this work, we focus on monocular vision-based semantic occupancy prediction, following the setting in [9], where a single image is used as input for each frame.

To evaluate the performance of semantic occupancy prediction, we employ the geometric Intersection over Union (IoU), per class semantic IoU and mean IoU over all semantic categories as the primary metrics. In addition, to evaluate the computational efficiency, we measure the inference speed in terms of frames per second (FPS), which reflects the practical efficiency and real-time capability of the model.

B. Implementation Details

For each frame, the input image is first cropped into a resolution of 1280×384 . Then, we adopt the image encoder from MaskDINO [48] with a ResNet-50 backbone as the pretrained image feature extractor, producing multi-scale image feature at downsampling ratios of $\{\frac{1}{4}, \frac{1}{8}, \frac{1}{16}, \frac{1}{32}, \frac{1}{64}\}$. The multi-scale image features are then fused into a unified representation at $\frac{1}{16}$ resolution using SECONDFPN [49]. The fused image feature is subsequently fed into depth and semantic predictors to obtain 2D depth distribution and semantic segmentation. Guided by the depth and semantic priors, the fused image feature is lifted into the 3D space through view transformation, producing a sparse volume feature at $\frac{1}{2}$ resolution of the target voxel grid. For the cascade sparse completion network, we

employ two hyper cross residual blocks in both the encoder and decoder. In the object contextual representation based mask decoder, the number of learnable queries is set to 100, and one cross-attention layer followed by one self-attention layer is applied. During voxel mask prediction, a learnable embedding is used to fill empty positions in the sparse volume feature, following the practice in [9].

During training, standard data augmentation strategies for depth estimation, semantic segmentation, and semantic occupancy prediction are applied. In addition, we employ a query denoising strategy with 20 denoising queries, together with an EMA scheme for model optimization. Model is trained using the AdamW optimizer with a learning rate of 4×10^{-4} for 20 epoches on 8 NVIDIA H100. For efficiency evaluation, all models are measured on an NVIDIA RTX 4090 using PyTorch fp32 backend with a batch size of 1. The FPS measurement follows the protocol in [30].

C. Main Results

We compare the proposed method with several representative and state-of-the-art 3D semantic occupancy prediction methods on the SemanticKITTI dataset, including MonoScene [26], TPVFormer [46], VoxFormer [28], OccFormer [27], SparseOcc [9] and ProtoOcc [31]. For performance comparison, the reported results of these methods are taken directly derived from their original papers. To ensure a fair evaluation of efficiency, we re-evaluate all models under their official configurations in a unified environment. Models with publicly available checkpoints are evaluated through direct inference. For methods without released weights, we retrain them from scratch following their reported configurations.

Table I presents an overall comparison on the SemanticKITTI validation set, including the image backbone, number of parameters, geometric IoU, mean IoU (mIoU) over all semantic classes and inference speed measured in FPS. As shown in the table, although using a relatively lightweight ResNet-50 based image backbone, our method achieves the highest mIoU and FPS among all compared approaches. In particular, compared with ProtoOcc, the proposed method improves mIoU by 7.42% while achieving a 57.81% increase in FPS. Note that the parameter counts and FPS of MonoScene,

TABLE II: 3D semantic occupancy prediction result of each semantic category on the SemanticKITTI validation set. The bold numbers indicate the best results. * represents these methods are adapted for the image inputs, which are implemented and reported in MonoScene [26].

Method	IoU	mIoU	Car	Bicycle	Motorcycle	Truck	Other-Vehicle	Person	Bicyclist	Motorcyclist	Road	Parking	Sidewalk	Other-Ground	Building	Fence	Vegetation	Trunk	Terrain	Pole	Trafficsign
LMSCNet* [23]	28.61	6.70	18.33	0.00	0.00	0.00	0.00	0.00	0.00	0.00	40.68	4.38	18.22	0.00	10.31	1.21	13.66	0.02	20.54	0.00	0.00
3DSketch* [26]	33.30	7.50	18.59	0.00	0.00	0.00	0.00	0.00	0.00	0.00	41.32	0.00	21.63	0.00	14.81	0.73	19.09	0.00	26.40	0.00	0.00
AICNet* [45]	29.59	8.31	14.71	0.00	0.00	4.53	0.00	0.00	0.00	0.00	43.55	11.97	20.55	0.07	12.94	2.52	15.37	2.90	28.71	0.06	0.00
JS3C-Net* [25]	38.98	10.31	15.03	0.00	0.00	4.41	6.15	0.67	0.27	0.00	50.49	11.94	23.74	0.07	15.03	3.94	18.11	4.33	26.86	3.77	1.45
MonoScene [26]	37.12	11.50	23.55	0.20	0.77	7.83	3.59	1.79	1.03	0.00	57.47	15.72	27.05	0.87	14.24	6.39	18.12	2.57	30.76	4.11	2.48
TPVFormer [46]	34.25	11.36	19.20	1.00	0.50	3.70	2.30	1.10	2.40	0.30	55.10	27.40	27.20	6.50	14.80	11.00	13.90	2.60	20.40	2.90	1.50
VoxFormer-S [28]	44.02	12.35	25.79	0.59	0.51	5.63	3.77	1.78	3.32	0.00	54.76	15.50	26.35	0.70	17.65	7.64	24.39	5.08	29.96	7.11	4.18
OccFormer [27]	36.67	13.46	25.09	0.81	1.19	25.53	8.52	2.78	2.82	0.00	58.85	19.61	26.88	0.31	14.40	5.61	19.63	3.93	33.62	4.26	2.86
SparseOcc [9]	36.50	13.12	25.09	0.78	0.89	18.07	8.94	3.68	0.62	0.00	59.59	20.44	29.68	0.47	14.40	6.73	18.89	3.46	31.06	3.89	2.60
ProtoOcc [31]	36.67	13.89	24.88	3.65	2.06	20.65	13.01	4.50	0.50	0.00	58.84	20.61	28.34	0.82	16.46	6.72	19.55	4.33	32.43	4.49	1.95
Ours	35.87	14.91	24.28	4.15	6.38	23.06	16.96	5.27	5.56	0.00	56.20	21.89	28.23	2.50	15.24	7.55	20.00	4.03	33.76	4.99	3.43

TABLE III: Ablation study for the impact of the three pruning ratios during the prediction pipeline. τ_s and τ_d represent respectively the semantic and depth uncertainty pruning ratio during view transformation. τ_p represent the pruning ratio during cascade sparse completion. Active voxels represent the number of features obtained from view transformation.

(τ_s, τ_d, τ_p)	IoU	mIoU	Active Voxels	FPS
(0.0, 0.0, 0.0)	35.84	14.50		7.8
(0.0, 0.0, 0.1)	35.59	14.71		9.3
(0.1, 0.1, 0.0)	36.71	15.10		8.2
(0.1, 0.1, 0.1)	35.87	14.91	45831	10.2
(0.1, 0.1, 0.3)	35.83	14.50		10.5
(0.3, 0.3, 0.1)	35.81	14.54	40967	10.4
(0.3, 0.3, 0.3)	36.35	14.52		10.8

TABLE IV: Ablation study for the impact of each proposed component.

Condition	IoU	mIoU	FPS
Baseline	35.87	14.91	10.1
w/o Distance-Aware Encoding	35.67	14.38	9.7
w/o Hyper-Cross Kernel	35.12	14.36	7.5
w/o Object Contextual Representation	35.21	14.25	10.4

TPVFormer and VoxFormer are not reported as their official implementations rely on legacy versions of PyTorch and CUDA that are incompatible with our evaluation environment.

Table II reports the per class IoU results of on the SemanticKITTI validation set, providing a fine-grained comparison of semantic occupancy prediction performance across different object and scenes. A closer inspection reveals that the overall improvement is primarily driven by consistent gains on small, sparse, and dynamic object categories, which are traditionally challenging for vision-based semantic occupancy prediction. In particular, the proposed method achieves higher

TABLE V: Ablation study for the impact of each training Strategy.

Condition	IoU	mIoU
Baseline	35.87	14.91
w/o Query Denoising	35.67	14.22
w/o Exponential Moving Average	35.98	13.34

IoU scores on Bicycle (4.15), Motorcycle (6.38), Other-Vehicle (16.96), Person (5.27), and Bicyclist (5.56) when compared with strong recent baselines such as ProtoOcc. These categories typically occupy limited spatial extents and exhibit complex geometric structures, and improvements on them contribute significantly to the overall mean IoU. Overall, the IoU results of each semantic category demonstrate that the proposed method enhances semantic occupancy prediction particularly on geometrically challenging categories, while maintaining competitive performance on other classes, resulting in a higher mIoU.

D. Ablation Study

In this section, we conduct ablation studies to analyze the contribution of individual components in the proposed framework, as well as the effects of key pruning hyperparameters and training strategies.

Table III presents the impact of different pruning thresholds settings on performance and efficiency of semantic occupancy prediction. The pruning strategy jointly considers three thresholds, τ_d , τ_s and τ_p , which correspond to semantic non-empty filtering at image level, depth uncertainty filtering based on the prefix sum of depth distributions, and empty voxel pruning during generative upsampling, respectively. As shown in Table III, the non-pruning setting (0, 0, 0) yields the lowest performance with a mIoU of 14.50 and a lowest FPS of 7.8. This confirms that lifting and decoding all positions

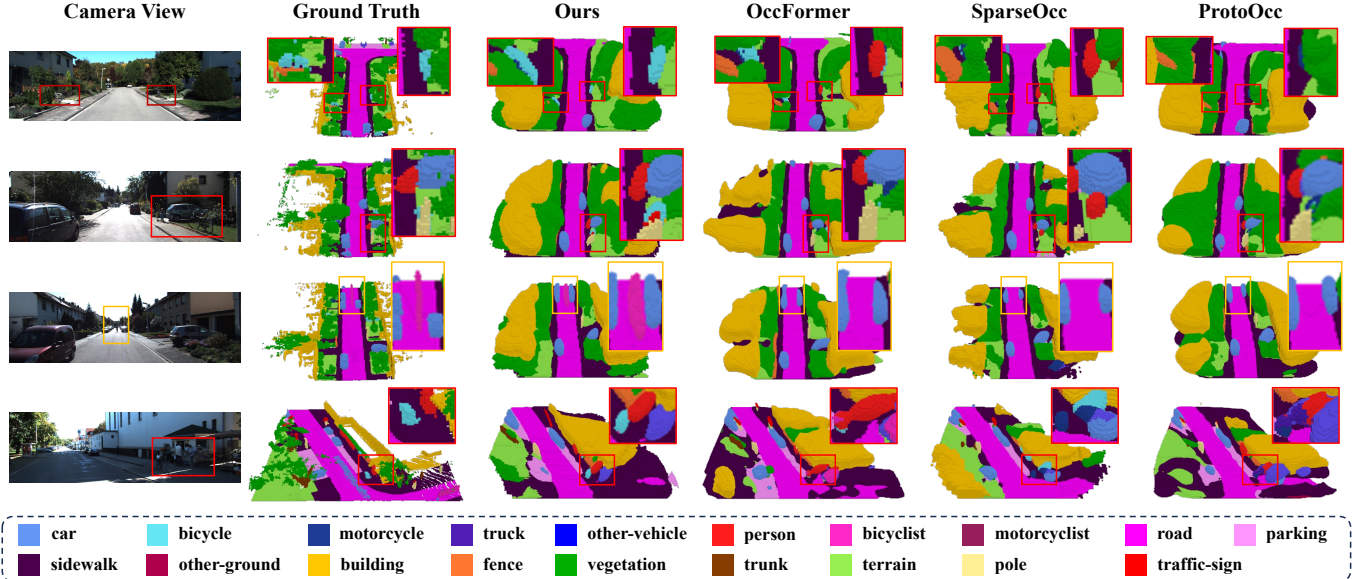


Fig. 6: Qualitative visualization results of our proposed SUG-Occ and others, along with the camera view and ground truth annotations. The zoom in region highlights the key region of interest.

introduces substantial redundancy and noise. Once pruning is enabled, both accuracy and speed exhibit clear and consistent improvements. Increasing the semantic and uncertainty thresholds (τ_s, τ_d) from (0, 0) to (0.1, 0.1) improves geometric IoU from 35.84 to 36.71 and mIoU from 14.50 to 15.10, together with a slight increase in FPS from 7.9 to 8.2. This improvement is accompanied by a reduction in the number of the active voxels from 59238 to 45831, indicating that filtering out image positions with a high confidence of being empty during view transformation leads to a cleaner and more compact sparse 3D representation. Furthermore, when enabling empty voxel pruning during generative upsampling by increasing τ_p from 0.0 to 0.1 while disabling image level pruning, FPS increases from 7.8 to 9.3 and mIoU slightly improves from 14.50 to 14.71. This suggests that active voxel control during the cascade generative upsampling stage not only improves computational efficiency but is also beneficial to performance. Combining the image level pruning with the upsampling stage pruning yields the most favorable trade-off between accuracy and efficiency, achieving an mIoU of 14.91 and a FPS of 10.2. When the pruning thresholds are further increased, the number of active voxels decreases only marginally, while both geometric IoU and mIoU begin to decline, indicating that overly aggressive pruning negatively affects semantic completeness.

Table IV presents an ablation study that analyzes the contribution of each component in the proposed methods. Starting from the full model as the baseline, we remove one component at a time and report the corresponding changes in geometric IoU, mIoU, and FPS. Removing the explicit distance encoding results in a noticeable decrease in mIoU by 0.53, indicating that explicit distance modeling plays an important role in preserving geometric structure during view transformation. Replacing the hyper cross convolution kernel with a stan-

dard cubic kernel leads to a clear reduction in FPS by 2.6, together with a decrease in mIoU by 0.55. This highlights the effectiveness of hyper cross sparse convolution in improving computational efficiency while maintaining representation quality. Excluding the object contextual representation module causes a significant drop in mIoU by 0.66, while FPS increase slightly by 0.3. This suggests that object context representation is beneficial for refining voxel-wise mask predictions while introducing only a small computational overhead. Overall, the results demonstrate that each proposed component contributes positively to the final performance, and their combination yields the best balance between accuracy and efficiency.

Table V reports the ablation study on the impact of the two training strategies employed in our framework, query denoising and exponential moving average. Removing the query denoising strategy results in a noticeable decrease in mIoU by 0.69, indicating that denoising queries facilitate more stable query learning and improved semantic discrimination during training. In parallel, excluding the exponential moving average strategy leads to a more pronounced performance reduction in mIoU by 1.57, suggesting that EMA plays a critical role in stabilizing model optimization and improving generalization. Overall, both query denoising and EMA contribute positively to the final performance, with EMA showing a stronger impact on model optimization stability and generalization ability.

E. Qualitative Visualization

Fig. 6 presents qualitative visualizations of the proposed method and the compared methods on the SemanticKITTI validation set. We select representative scenes and visualize the predicted 3D semantic occupancy results alongside the corresponding camera views and ground truth annotations. Overall, our method produces more complete and structurally

consistent semantic occupancy predictions, particularly for small, dynamic, and thin structured objects.

As illustrated in the zoomed regions, our approach shows clear advantages in predicting classes like persons, bicycle, and motorcycle. In contrast, the compared methods exhibit object missing or semantic confusion to varying degrees across different scenarios. For example, in the third scene, all the compared methods fail to detect a bicycle located farther away in the middle of the road. In the second scene, although a person, a bicycle, and a car are present on the right side of the camera view, some compared methods miss the bicycle while others incorrectly predict its semantics. Such errors could pose potential safety risks to autonomous driving system. In comparison, our proposed method handle these challenging scenes more effectively by consistently predicting clearer object extents and more accurate semantic labels.

V. CONCLUSION AND DISCUSSION

This work introduces SUG-Occ, a real-time 3D semantic occupancy prediction network that utilizes semantics and uncertainty guided sparse learning with explicit distance encoding. By integrating semantic and depth priors to selectively lift informative image projections during view transformation, the proposed method constructs a robust and compact sparse 3D representation, effectively reducing redundancy while preserving geometric and semantic consistency. Built upon this sparse representation, a lightweight cascade sparse completion module efficiently reconstructs scene geometry and semantics via hyper cross sparse convolution, generative upsampling and adaptive pruning. To further refine semantic occupancy prediction, an object contextual representation based mask decoder aggregates global semantic context from sparse features and performs lightweight query-context interactions, avoiding expensive dense voxel wise attention while maintaining strong semantic reasoning capability. Extensive experiments demonstrates on the SemanticKITTI dataset that the proposed method achieves state-of-the-art performance while significantly improving inference efficiency, enabling real-time deployment in autonomous driving system.

The primary limitation of this work lies in its reliance on single-frame camera inputs, without leveraging temporal information or multi-vehicle collaborative cues. Future work could integrate temporal modeling, multi-modal sensory inputs, and collaborative perception among multiple agents to further enhance the performance and scalability of the proposed framework.

REFERENCES

- [1] H. Xu, J. Chen, S. Meng, Y. Wang, and L.-P. Chau, “A survey on occupancy perception for autonomous driving: The information fusion perspective,” *arXiv preprint arXiv:2405.05173*, 2024.
- [2] M.-H. Guo, C.-Z. Lu, Q. Hou, Z. Liu, M.-M. Cheng, and S.-M. Hu, “Segnext: Rethinking convolutional attention design for semantic segmentation,” *Advances in neural information processing systems*, vol. 35, pp. 1140–1156, 2022.
- [3] L.-C. Chen, G. Papandreou, I. Kokkinos, K. Murphy, and A. L. Yuille, “Deeplab: Semantic image segmentation with deep convolutional nets, atrous convolution, and fully connected crfs,” *IEEE transactions on pattern analysis and machine intelligence*, vol. 40, no. 4, pp. 834–848, 2017.
- [4] Y. Yan, Y. Mao, and B. Li, “Second: Sparsely embedded convolutional detection,” *Sensors*, vol. 18, no. 10, p. 3337, 2018.
- [5] A. H. Lang, S. Vora, H. Caesar, L. Zhou, J. Yang, and O. Beijbom, “Pointpillars: Fast encoders for object detection from point clouds,” in *Proceedings of the IEEE/CVF conference on computer vision and pattern recognition*, 2019, pp. 12 697–12 705.
- [6] Z. Li, W. Wang, H. Li, E. Xie, C. Sima, T. Lu, Q. Yu, and J. Dai, “Bevformer: learning bird’s-eye-view representation from lidar-camera via spatiotemporal transformers,” *IEEE Transactions on Pattern Analysis and Machine Intelligence*, 2024.
- [7] Z. Liu, H. Tang, A. Amini, X. Yang, H. Mao, D. Rus, and S. Han, “Bevfusion: Multi-task multi-sensor fusion with unified bird’s-eye view representation,” *arXiv preprint arXiv:2205.13542*, 2022.
- [8] J. Philion and S. Fidler, “Lift, splat, shoot: Encoding images from arbitrary camera rigs by implicitly unprojecting to 3d,” in *European conference on computer vision*. Springer, 2020, pp. 194–210.
- [9] P. Tang, Z. Wang, G. Wang, J. Zheng, X. Ren, B. Feng, and C. Ma, “Sparseocc: Rethinking sparse latent representation for vision-based semantic occupancy prediction,” in *Proceedings of the IEEE/CVF Conference on Computer Vision and Pattern Recognition*, 2024, pp. 15 035–15 044.
- [10] A.-Q. Cao, A. Dai, and R. De Charette, “Pasco: Urban 3d panoptic scene completion with uncertainty awareness,” in *Proceedings of the IEEE/CVF Conference on Computer Vision and Pattern Recognition*, 2024, pp. 14 554–14 564.
- [11] H. Liu, Y. Chen, H. Wang, Z. Yang, T. Li, J. Zeng, L. Chen, H. Li, and L. Wang, “Fully sparse 3d occupancy prediction,” in *European Conference on Computer Vision*. Springer, 2024, pp. 54–71.
- [12] J. Wang, Z. Liu, Q. Meng, L. Yan, K. Wang, J. Yang, W. Liu, Q. Hou, and M.-M. Cheng, “Opus: occupancy prediction using a sparse set,” *Advances in Neural Information Processing Systems*, vol. 37, pp. 119 861–119 885, 2024.
- [13] C. Reading, A. Harakeh, J. Chae, and S. L. Waslander, “Categorical depth distribution network for monocular 3d object detection,” in *Proceedings of the IEEE/CVF conference on computer vision and pattern recognition*, 2021, pp. 8555–8564.
- [14] J. Huang, G. Huang, Z. Zhu, Y. Ye, and D. Du, “Bevdet: High-performance multi-camera 3d object detection in bird-eye-view,” *arXiv preprint arXiv:2112.11790*, 2021.
- [15] J. Huang and G. Huang, “Bevdet4d: Exploit temporal cues in multi-camera 3d object detection,” *arXiv preprint arXiv:2203.17054*, 2022.
- [16] Y. Li, Z. Ge, G. Yu, J. Yang, Z. Wang, Y. Shi, J. Sun, and Z. Li, “Bevdepth: Acquisition of reliable depth for multi-view 3d object detection,” in *Proceedings of the AAAI conference on artificial intelligence*, vol. 37, no. 2, 2023, pp. 1477–1485.
- [17] Y. Wei, L. Zhao, W. Zheng, Z. Zhu, J. Zhou, and J. Lu, “Surroundocc: Multi-camera 3d occupancy prediction for autonomous driving,” in *Proceedings of the IEEE/CVF International Conference on Computer Vision (ICCV)*, October 2023, pp. 21 729–21 740.
- [18] S. Song, F. Yu, A. Zeng, A. X. Chang, M. Savva, and T. Funkhouser, “Semantic scene completion from a single depth image,” in *Proceedings of the IEEE conference on computer vision and pattern recognition*, 2017, pp. 1746–1754.
- [19] J. Behley, M. Garbade, A. Milioto, J. Quenzel, S. Behnke, C. Stachniss, and J. Gall, “SemanticKITTI: A Dataset for Semantic Scene Understanding of LiDAR Sequences,” in *Proc. of the IEEE/CVF International Conf. on Computer Vision (ICCV)*, 2019.
- [20] J. Behley, M. Garbade, A. Milioto, J. Quenzel, S. Behnke, J. Gall, and C. Stachniss, “Towards 3D LiDAR-based semantic scene understanding of 3D point cloud sequences: The SemanticKITTI Dataset,” *The International Journal on Robotics Research*, vol. 40, no. 8-9, pp. 959–967, 2021.
- [21] Y. Li, S. Li, X. Liu, M. Gong, K. Li, N. Chen, Z. Wang, Z. Li, T. Jiang, F. Yu, et al., “Sscbench: Monocular 3d semantic scene completion benchmark in street views,” *arXiv preprint arXiv:2306.09001*, 2023.
- [22] X. Tian, T. Jiang, L. Yun, Y. Mao, H. Yang, Y. Wang, Y. Wang, and H. Zhao, “Occ3d: A large-scale 3d occupancy prediction benchmark for autonomous driving,” *Advances in Neural Information Processing Systems*, vol. 36, 2024.
- [23] L. Roldão, R. de Charette, and A. Verroust-Blondet, “Lmscnet: Lightweight multiscale 3d semantic completion,” in *2020 International Conference on 3D Vision (3DV)*, 2020, pp. 111–119.
- [24] R. Cheng, C. Agia, Y. Ren, X. Li, and L. Bingbing, “S3cnet: A sparse semantic scene completion network for lidar point clouds,” in *Proceedings of the 2020 Conference on Robot Learning*, ser. Proceedings of Machine Learning Research, J. Kober, F. Ramos, and C. Tomlin, Eds., vol. 155. PMLR, 16–18 Nov 2021, pp. 2148–2161.

[25] X. Yan, J. Gao, J. Li, R. Zhang, Z. Li, R. Huang, and S. Cui, “Sparse single sweep lidar point cloud segmentation via learning contextual shape priors from scene completion,” in *Proceedings of the AAAI Conference on Artificial Intelligence*, vol. 35, no. 4, 2021, pp. 3101–3109.

[26] A.-Q. Cao and R. de Charette, “Monoscene: Monocular 3d semantic scene completion,” in *Proceedings of the IEEE/CVF Conference on Computer Vision and Pattern Recognition (CVPR)*, June 2022, pp. 3991–4001.

[27] Y. Zhang, Z. Zhu, and D. Du, “Occformer: Dual-path transformer for vision-based 3d semantic occupancy prediction,” in *Proceedings of the IEEE/CVF International Conference on Computer Vision (ICCV)*, October 2023, pp. 9433–9443.

[28] Y. Li, Z. Yu, C. Choy, C. Xiao, J. M. Alvarez, S. Fidler, C. Feng, and A. Anandkumar, “Voxformer: Sparse voxel transformer for camera-based 3d semantic scene completion,” in *2023 IEEE/CVF Conference on Computer Vision and Pattern Recognition (CVPR)*, 2023, pp. 9087–9098.

[29] X. Tan, W. Wu, Z. Zhang, C. Fan, Y. Peng, Z. Zhang, Y. Xie, and L. Ma, “Geocc: Geometrically enhanced 3d occupancy network with implicit-explicit depth fusion and contextual self-supervision,” *IEEE Transactions on Intelligent Transportation Systems*, 2025.

[30] D. Chen, J. Fang, W. Han, X. Cheng, J. Yin, C. Xu, F. S. Khan, and J. Shen, “Alloc: Adaptive lifting-based 3d semantic occupancy and cost volume-based flow predictions,” in *Proceedings of the IEEE/CVF International Conference on Computer Vision*, 2025, pp. 4156–4166.

[31] J. Kim, C. Kang, D. Lee, S. Choi, and J. W. Choi, “Protoocc: Accurate, efficient 3d occupancy prediction using dual branch encoder-prototype query decoder,” in *Proceedings of the AAAI Conference on Artificial Intelligence*, vol. 39, no. 4, 2025, pp. 4284–4292.

[32] B. Liu, M. Wang, H. Foroosh, M. Tappen, and M. Pensky, “Sparse convolutional neural networks,” in *Proceedings of the IEEE conference on computer vision and pattern recognition*, 2015, pp. 806–814.

[33] B. Graham and L. Van der Maaten, “Submanifold sparse convolutional networks,” *arXiv preprint arXiv:1706.01307*, 2017.

[34] C. Choy, J. Gwak, and S. Savarese, “4d spatio-temporal convnets: Minkowski convolutional neural networks,” in *Proceedings of the IEEE/CVF conference on computer vision and pattern recognition*, 2019, pp. 3075–3084.

[35] J. Gwak, C. Choy, and S. Savarese, “Generative sparse detection networks for 3d single-shot object detection,” in *European conference on computer vision*. Springer, 2020, pp. 297–313.

[36] J. Liu, Y. Chen, X. Ye, Z. Tian, X. Tan, and X. Qi, “Spatial pruned sparse convolution for efficient 3d object detection,” *Advances in neural information processing systems*, vol. 35, pp. 6735–6748, 2022.

[37] Y. Chen, Y. Li, X. Zhang, J. Sun, and J. Jia, “Focal sparse convolutional networks for 3d object detection,” in *Proceedings of the IEEE/CVF conference on computer vision and pattern recognition*, 2022, pp. 5428–5437.

[38] H. Liu, Y. Teng, T. Lu, H. Wang, and L. Wang, “Sparsebev: High-performance sparse 3d object detection from multi-camera videos,” in *Proceedings of the IEEE/CVF international conference on computer vision*, 2023, pp. 18 580–18 590.

[39] L. Chambon, E. Zablocki, M. Chen, F. Bartoccioni, P. Pérez, and M. Cord, “Pointbev: A sparse approach for bev predictions,” in *Proceedings of the IEEE/CVF conference on computer vision and pattern recognition*, 2024, pp. 15 195–15 204.

[40] F. Chollet, “Xception: Deep learning with depthwise separable convolutions,” in *Proceedings of the IEEE conference on computer vision and pattern recognition*, 2017, pp. 1251–1258.

[41] Y. Yuan, X. Chen, and J. Wang, “Object-contextual representations for semantic segmentation,” in *European conference on computer vision*. Springer, 2020, pp. 173–190.

[42] F. Li, H. Zhang, S. Liu, J. Guo, L. M. Ni, and L. Zhang, “Dn-detr: Accelerate detr training by introducing query denoising,” in *Proceedings of the IEEE/CVF conference on computer vision and pattern recognition*, 2022, pp. 13 619–13 627.

[43] D. Morales-Brottons, T. Vogels, and H. Hendrikx, “Exponential moving average of weights in deep learning: Dynamics and benefits,” *arXiv preprint arXiv:2411.18704*, 2024.

[44] M. Berman, A. R. Triki, and M. B. Blaschko, “The lovasz-softmax loss: A tractable surrogate for the optimization of the intersection-over-union measure in neural networks,” in *Proceedings of the IEEE conference on computer vision and pattern recognition*, 2018, pp. 4413–4421.

[45] X. Chen, K.-Y. Lin, C. Qian, G. Zeng, and H. Li, “3d sketch-aware semantic scene completion via semi-supervised structure prior,” in *Proceedings of the IEEE/CVF Conference on Computer Vision and Pattern Recognition*, 2020, pp. 4193–4202.

[46] Y. Huang, W. Zheng, Y. Zhang, J. Zhou, and J. Lu, “Tri-perspective view for vision-based 3d semantic occupancy prediction,” in *Proceedings of the IEEE/CVF Conference on Computer Vision and Pattern Recognition (CVPR)*, June 2023, pp. 9223–9232.

[47] A. Geiger, P. Lenz, and R. Urtasun, “Are we ready for autonomous driving? the kitti vision benchmark suite,” in *2012 IEEE conference on computer vision and pattern recognition*. IEEE, 2012, pp. 3354–3361.

[48] F. Li, H. Zhang, H. Xu, S. Liu, L. Zhang, L. M. Ni, and H.-Y. Shum, “Mask dino: Towards a unified transformer-based framework for object detection and segmentation,” in *Proceedings of the IEEE/CVF conference on computer vision and pattern recognition*, 2023, pp. 3041–3050.

[49] V. A. Sindagi, Y. Zhou, and O. Tuzel, “Mvx-net: Multimodal voxelnet for 3d object detection,” in *2019 International Conference on Robotics and Automation (ICRA)*. IEEE, 2019, pp. 7276–7282.